A Texture-based Segmentation Method for Improved Iris Recognition

Xiaojing Yuan, Ilyas Uyanik
Engineering Technology Department, University of Houston, Texas, United States

Abstract – Many research and algorithms have been developed for iris recognition in recent years due to advances in imaging acquisition and processing and renewed emphasis in biometric based security measure, given that iris recognition is still the most accurate biometrics used in security identification. The advances in imaging acquisition enabled more accurate and realistic iris images, while introducing new challenges for iris recognition due to reflection, which negatively affected the performance of the traditional segmentation methods used for iris recognition. In this paper, we present a new iris segmentation and pattern extraction algorithm that achieves high performance with or without reflection. The segmentation based iris recognition system developed in the paper streamlined while set of analysis algorithms for iris recognition from image preprocessing, feature extraction, enrollment, to recognition. The system achieved perfect recognition rate when tested on well-known iris recognition databases CASIA-IrisV1 and CASIA-IrisV3, provided by the Chinese Academy of Sciences.

Key Words – iris recognition, iris segmentation, normalization, 2D Gabor filter bank, texture feature extraction.

I. Introduction

Reliable and automatic recognition of individuals(a.k.a., personal identification) has long been a goal in law enforcement and security applications. As in other pattern recognition systems, the key challenge remains as to be able to model the relationship between interclass and intra-class variability accurately so that objects can be reliably classified with low error rate [1, 2].

Iris patterns became attractive as an alternative approach for reliable visual identification of a person with the advances in imaging acquisition. Using iris pattern as a biometric security measure has several advantages over other biometric measures such as face, finger-prints, voice-prints, or gait signature. First of all, the iris pattern variability among different person is enormous, thus satisfies the unique identification requirement. Secondly, as an internal, yet externally visible organ of the eye, the iris is well protected from the environment and stable over time. The extraordinary structure of the human iris provides abundant texture and spatial patterns that are unique to each individual. All these remain remarkably stable over many decades, making the iris pattern more reliable for personal identification [3]. Thirdly, from analysis perspective, as a planar object, the iris image is relatively insensitive to angle of illumination. Furthermore, changes in viewing angle cause only affine transformations. Even the non-affine pattern distortion caused by pupillary dilation is readily reversible [4]. Lastly, it is relatively easy to localize eyes in faces. The distinctive annular shape of the iris further facilitates reliable and precise isolation of it from the eye [5]. All these features make the iris recognition as personal identification more accurate and reliable as compared with using other biometric measures.

Furthermore, with advances in imaging acquisition, accurate iris images can be captured rapidly from a distance of about one meter nowadays, with ongoing research to increase that distance so that iris recognition can be extended to applications such as airport security monitoring from access security screening. Moreover, faster and efficient storage mechanism and search algorithms enabled searching for a match of a specific iris pattern in very large databases (and getting bigger) without incurring any false matches despite a huge number of possibilities. It is no surprise that given the increasing demand of more security and the advances in image acquisition and analysis iris recognition is getting renewed attention.

In this paper, we present our new segmentation method based iris recognition system that can deal with traditional iris image as well as more realistic iris image. Section II presents the framework of our iris recognition system that incorporates functions from image preprocessing, iris segmentation, feature extraction, enrollment, to recognition. Section III presents our segmentation method that extracts iris-pupil and iris-sclera boundary. Section IV describes the details of texture feature extraction based on two-

Corresponding Author: Xiaojing Yuan, Email: xyuan@uh.edu

dimensional (2D) Gabor filter bank, including the normalization and image enhancement processes that ensure features extracted from iris images taken from different condition are comparable. Section V presents the iris database we use, the experiment setup and results. Conclusions will be drawn in Section VI with directions for future work.

II. Iris Recognition System Architecture

As shown in Figure 1, two main stages are necessary for any iris recognition system to function properly after iris images are acquired: enrollment and recognition. Each stage shares some common functions such as image pre-processing, iris segmentation, image enhancement, and feature pattern extraction. After extracting iris feature pattern, different actions are taken for enrollment and recognition stages. For enrollment, the extracted feature pattern is saved into the database, with pointers established to link to its corresponding raw iris image. For recognition, the extracted iris feature pattern will be compared to the pattern stored in the database using Euclidian distance, resulting in a similarity value. These similarity values will be ranked and the iris image with maximum similarity value or a set of iris images with similarity values above user defined threshold will be returned as the matched results. If all similarity values between the incoming iris image and those in the database are less than the threshold, the system will return "no match" result, and trigger the enrollment process automatically.

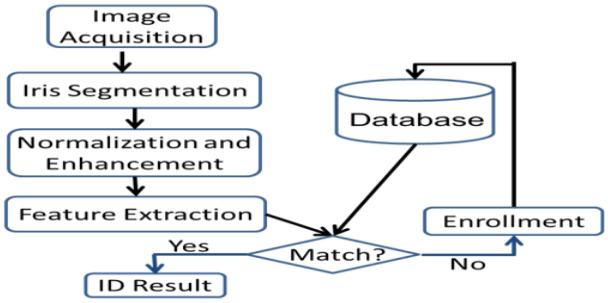

Fig. 1 Iris recognition system architecture

III. Image Preprocessing and Iris Segmentation

There are many pre-processing steps that are needed for any iris recognition system given that most iris images are acquired in the RGB color space, with little or none light and noise control. These include color mapping from RGB (red, green, and blue) to HIS (hue, saturation, and intensity) color space, noise reduction and artifacts (such as dense and intrusive eyelashes) removing.

Figure 2 shows iris images from the CASIA-IrisV1 database (left) and the CASIA-IrisV3 database (right). The iris locates between the sclera and the pupil. In order to extract iris feature pattern, iris needs to be segmented out by identifying the boundaries between iris-pupil and iris-sclera, which is not trivial. As shown in Figure 2, the iris images from CASIA-IrisV3 dataset (right) have light reflection in the pupil, making them more realistic; while the iris images from CASIA-IrisV1 dataset (left) have the light refection removed beforehand. The technical challenge lies in answering the question of "how can we accurately and efficiently localize the iris boundary without additional pre-processing step to remove the light reflection in the pupil?"[14] An efficient and accurate iris segmentation algorithm or mechanism for CASIA-IrisV3 dataset can be easily adapted for other realistic iris database such as UBIRIS-V2 and Iris Challenge Evaluation dataset used in 2005 (ICE2005) and 2006 (ICE2006).

As shown in Figure 2, iris segmentation requires identification of boundaries between the iris and pupil (inner boundary) and iris and sclera (outer boundary). In the next subsections, we will present in detail both boundary localization and illustrate the difference between CASIA-IrisV1 and CASIA-IrisV3.

3.1 Iris-Pupil Boundary Localization

For iris image from the CASIA-IrisV1 dataset, the boundary between iris and pupil can be identified simple by applying any edge detection algorithm since the pupil area has homogenous low intensity value (usually the lowest intensity value in the whole image). Figure 3 shows the process of iris-pupil boundary localization with a sample iris image from CASIA-IrisV1.

Using I(x,y) to represent the pixel intensity in the image, in which x and y are the Cartesian coordination of the pixel, we identify the minimum intensity value (min(I(x,y)) and its location in the iris image. For iris images from CASIA-IrisV1dataset, such a pixel always locates in the pupil. Figure 3 (b) shows the heat-map of each pixel based on its intensity value for the sample iris image. Using the location of the pixel with minimum intensity value as the new origins (as pointed by arrows in Figure 3 (c)), a threshold value of (min (I(x,y))+N) is then used to identify the boundary between the iris-pupil based on the histogram in the x- and y- direction respectively. N is empirically chosen. Note that instead of counting.

Fig. 2 Iris Image examples from CASIA-IrisV1 (left) and CASIA-IrisV3 (right) databases

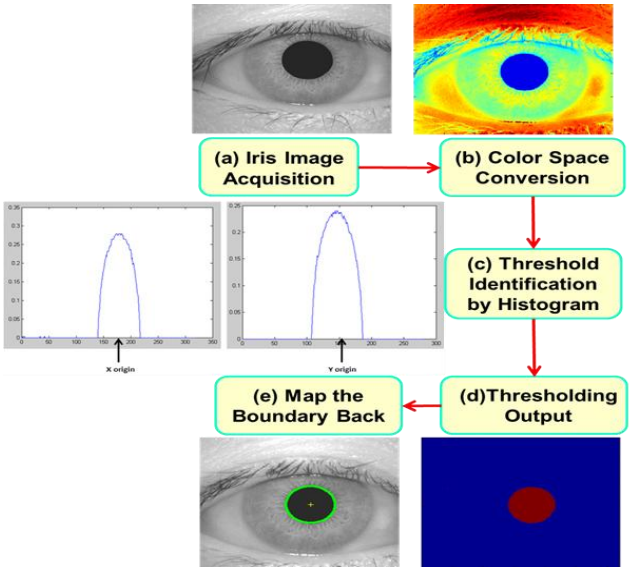

Fig. 3 Iris-Pupil Boundary Localization: CASIA-IrisV1

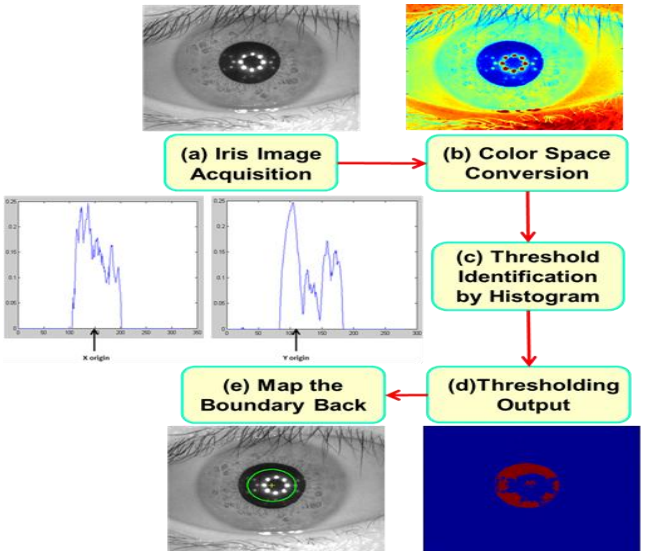

Fig. 4 Iris-Pupil Boundary Localization: CASIA-IrisV3

based on the pixel intensity directly, Figure 3 (c) shows the percentage of the pixels below the threshold in each direction. Figure 3 (d) shows the extracted pupil area using the simple thresholding methods based on the threshold identified. Figure 3 (e) illustrated the iris-pupil boundary in green circle after mapping the identified boundary back to the original iris image

For iris images from the CASIA–IrisV3 dataset, even though the iris pattern remains clear, the iris-pupil boundary localization is much more difficult due to the light reflection within the pupil. Figure 4 shows the results when applying the same algorithm to iris image from CASIA-IrisV3 dataset. Because of the reflection captured in the pupil area, it does not provide homogenous low intensity area. Hence, the accuracy of identifying the iris-pupil boundary using histogram decreases, as shown in Figure 4(d) and (e).

To address these issues, we introduced two basic mathematical morphology (MM) operations: dilation and erosion, before threshold identification step. MM theory and techniques are used in the analysis and processing of geometrical spatial structures based on set theory, lattice theory and topology. Used in imaging processing, the MM operations consider the image as a set of pixel values (primary set), and apply pre-defined shape (secondary set) to see whether it fits or misses the region of interest (object) in the primary set. The advantage of basic MM operations is that they are translation invariant.

The dilation operation of a secondary set B on a primary set A is defined by $A \oplus B = \bigcup_{b \in B} A_b$. In Matlab, the dilation operation is implemented so that the value of the output pixel is the maximum value of all the pixels in the input pixel's neighborhood, resulting in expanded boundary.

Similarly, the erosion operation is defined by $A \ominus B = \{z \in E | B_z \subseteq A\}$, where B_z is the translation of B by the vector z, i.e., $B_z = \{b + z | b \in B\}, \forall z \in E$. In Matlab, the erosion operation is implemented so that the value of the output pixel is the minimum value of all the pixels in

the input pixel's neighborhood, resulting in shrank boundary.

To address the light reflection in the pupil, we first applied the dilation operation with the secondary set B chosen as an open disk with radius of 3, with its center moved around the identified boundary as shown in Figure 5(a). Result is shown in Figure 5(b), including the resulting binary image and the resulting image after the boundary is mapped back to the original iris image. Afterwards, erosion operation is applied to shrink the boundary with the radium of the open disk representing the secondary set B chosen as 2, with results shown in Figure 5 (c). Figure 5 also compares the histogram from original algorithm with that after the dilation and erosion operations. The resulting histogram shows smooth region within the pupil, indicating intensity homogeneity. The histogram is used to identify the accurate iris-pupil boundary as before, with resulting boundary shown in Figure 5 (c).

3.2 Iris-Sclera Boundary Localization

After identifying the boundary between the iris-pupil, boundary between the iris and sclera needs to be identified. It is generally agreed that the iris-sclera boundary localization is more difficult than iris-pupil boundary identification [6] because of the low contrast between iris and sclera and intensity heterogeneity of iris. Various segmentation algorithms [7], including active contour and Hough transform, have been applied to iris-sclera boundary detection. The main drawback of these algorithms is their computational complexity, resulting in more computation time and memory space.

In our iris recognition system, we identify the iris-sclera boundary by applying the Sobel operator. A discrete differentiation operator, the Sobel operator convolving the image with a small, separable, and integer valued filter in horizontal and vertical direction to approximate the gradient of the image intensity function. Compared with other edge detection algorithms, it is computationally inexpensive. The gradient approximation Sobel operator produces is crude, i.e., the identified edge or boundary is not precise. However, it is good enough for iris-sclera boundary identification since even high-noised imperfect iris images do not have high- frequency variations. Figure 6 shows the iris-sclera boundary identification result, with identified iris-pupil boundary, for a sample iris image from CASIA-IrisV3 dataset.

IV. Image Enhancement and Feature Extraction

4.1 Iris Normalization and Image Enhancement

Iris images are increasingly acquired without strict constraints, resulting in more intra-class variations caused by illumination (camera gain, contrast settings), position and pose, and other external noise. To enable comparison of iris images taken under different conditions, the iris normalization process tries to minimize intra-class variance without compromise inter-class variance (difference from

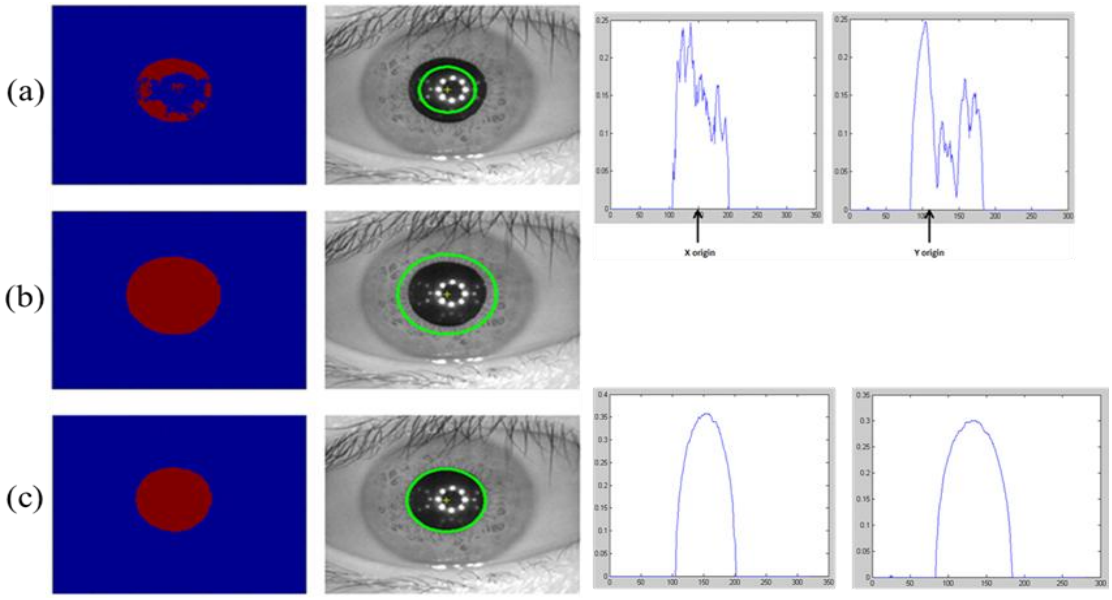

Fig. 5 Iris-Pupil Boundary Localization after MM operations: (a) original, (b) dilation, and (c) erosion

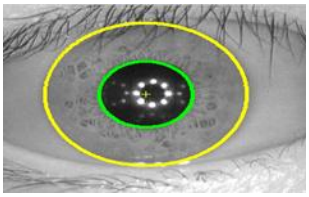

Fig. 6 Iris-Sclera boundary identification result of a sample iris image from CASIA-IrisV3 dataset

person to person) and outputs a normalized iris sheet with the same constant dimensions. The normalization step ensures that the characteristic features of iris pattern extracted will be the same at the same spatial location regardless of how the original iris images were acquired.

In our iris recognition system, we use Daugman model [5] for the normalization process. The Daugman model maps each pixel within the segmented iris region to a pair of polar coordinates (r, θ), in which r $\in$ [0,1] and θ$\in$[0,2π]. The mapping process and equation are shown in Figure 7, in which the normalized iris sheet is displayed as a rectangular image with size M*N, with the radial coordinate on the vertical axis, and the angular coordinate on the horizontal axis [9].

By taking the pupil dilation and size inconsistence (intra-class variation) into consideration, the Daugman method models the iris region as a flexible rubber sheet anchored at the iris boundary with the pupil center as the reference point, resulting in a normalized representation of iris with constant dimensions. In our experiment, we quantize the radius in the range of [1, 64] and the orientation θ in the range of [1-512], resulting in normalized iris sheet with constant dimension of 512 X 64. Figure 8 shows an example of the normalized iris sheet of the sample iris image from CASIA-IrisV3 dataset.

After mapping the extracted iris region from Cartesian representation I(x,y) to polar representation I(r, θ), a low pass Gaussian filter with window size of MxM is applied to the normalized iris sheet first. The intensity of the central pixel within the window of the Gaussian filter is replaced by the mean intensity of the pixels within the window, resulting in the iris background bias sheet (Figure 8 (b)). Then, the enhanced iris sheet is obtained by subtracting the iris background bias sheet from the normalized iris sheet (Figure 8 (c)).

4.2 Iris Texture Feature Pattern Extraction

Many feature extraction algorithms have been proposed to extract unique and invariant features from the iris patterns, including variations of Gabor, wavelet filter [10-13] extracting texture and spatial features. Gabor filters are well known as texture feature extraction method that produces feature invariant to scaling, shift, and rotation [8]. Equation (1) is used to compute Gabor filter response of a two-dimension (2-D) image in the Cartesian domain.

$$g(x,y) = \frac{1}{2\pi\sigma_x\sigma_y}\exp\left(-\frac{1}{2}\left(\frac{x_1^2}{\sigma_x^2}+\frac{y_1^2}{\sigma_y^2}\right)+2\pi f x_1\right) \quad (1)$$

in which $x_1 = xcos\vartheta + ysin\vartheta$ and $y_1 = -xcos\vartheta + ycos\vartheta$, and f is the frequency and θ is the orientation of the filter.

Gabor filter responses can be divided into two parts: the real part and the imaginary part, as shown in Equation (2)-(4).

$$g(x,y) = g^e(x,y) + jxg^o(x,y) \quad (2)$$

$$g^e(x,y) = \frac{1}{2\pi\sigma_y\sigma_x}\exp[-\frac{1}{2}(\frac{x_1^2}{\sigma_y^2}+\frac{y_1^2}{\sigma_y^2})]\cos 2\pi F x_1) \quad (3)$$

$$g^0(x,y) = \frac{1}{2\pi\sigma_y\sigma_x}\exp[-\frac{1}{2}(\frac{x_1^2}{\sigma_y^2}+\frac{y_1^2}{\sigma_y^2})]\sin 2\pi F x) \quad (4)$$

In our iris recognition system, we use 2-D Gabor filter with five central radial frequencies f: ([0.157, 0.346, 0.691, 1.414, 2.827]) and four orientations ϑ: ([0 45 90 135]). Each enhanced normalized iris sheet is divided into eight equal sized patches (32x64). Each patch then is fed into the Gabor filter bank and produces 20 filter responses with the same size. For the filter response of each patch, the average absolute deviation (AAD) defined in Equation (3) is used to represent its texture feature:

$$E = \frac{1}{N}(\sum_N |G(x,y) - \mu|) \quad (5)$$

in which N is the size of the patch and its filter response, μ is mean filter response of the patch, and G(x,y) is the Gabor filter response coefficient at pixel (x, y).

For one iris image, we get a feature vector with 160 ADD values, representing the texture pattern of the enhanced normalized iris sheet. Figure 10 shows the Gabor filter bank based texture feature extraction and a sample feature vector with length of 160 and ADD values ranges from 0 to 0.03. The extracted feature vector for the iris image will be stored into the database for enrollment or compared to the texture feature vectors for iris images already in the database for matching and recognition.

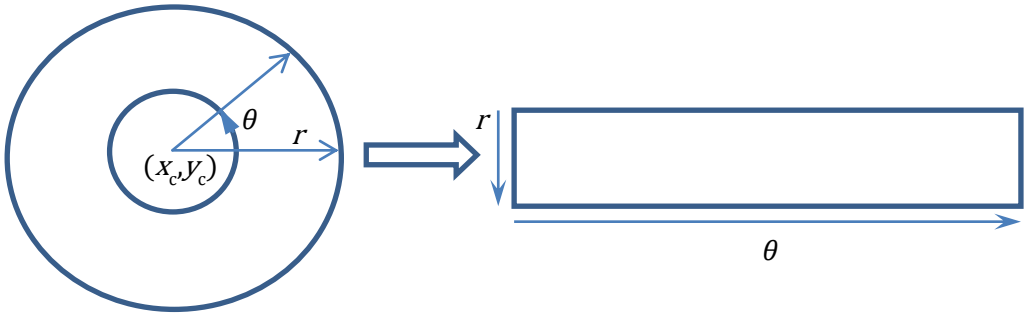

$$I(x,y) \rightarrow I(r,\theta)$$
$$r = \sqrt{(x-x_c)^2 + (y-y_c)^2}\,,\ 0 \le r \le r_{max}$$
$$\theta = tan^{-1}\left(\frac{y-y_c}{x-x_c}\right),$$
$$(x_c,\ y_c)\ is\ the\ Cartesian\ coordination\ of\ the\ center\ pixel.$$

Fig. 7 Daugman Model based normalization process and equations

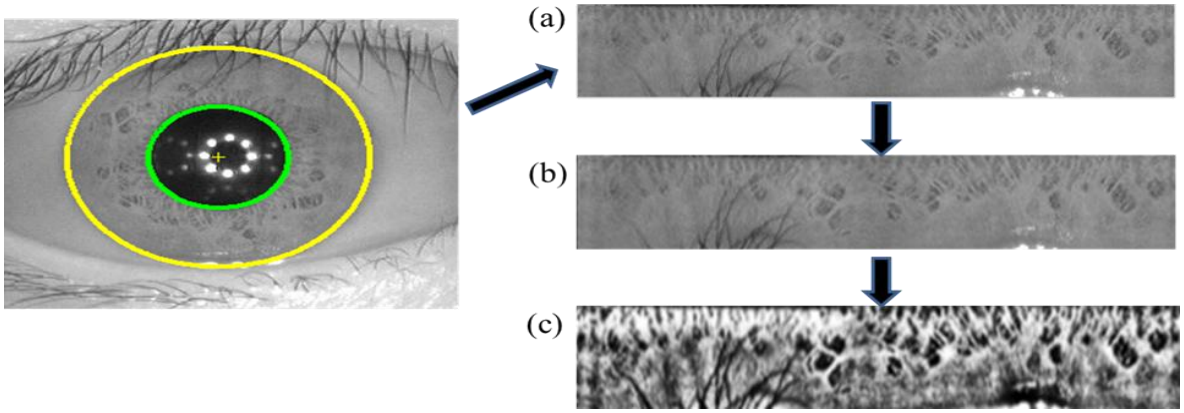

Fig. 8 (a) Normalized iris sheet from Daugman normalization of a sample iris image from CASIA-IrisV3 dataset; (b) iris background bias sheet; and (c) enhanced iris sheet

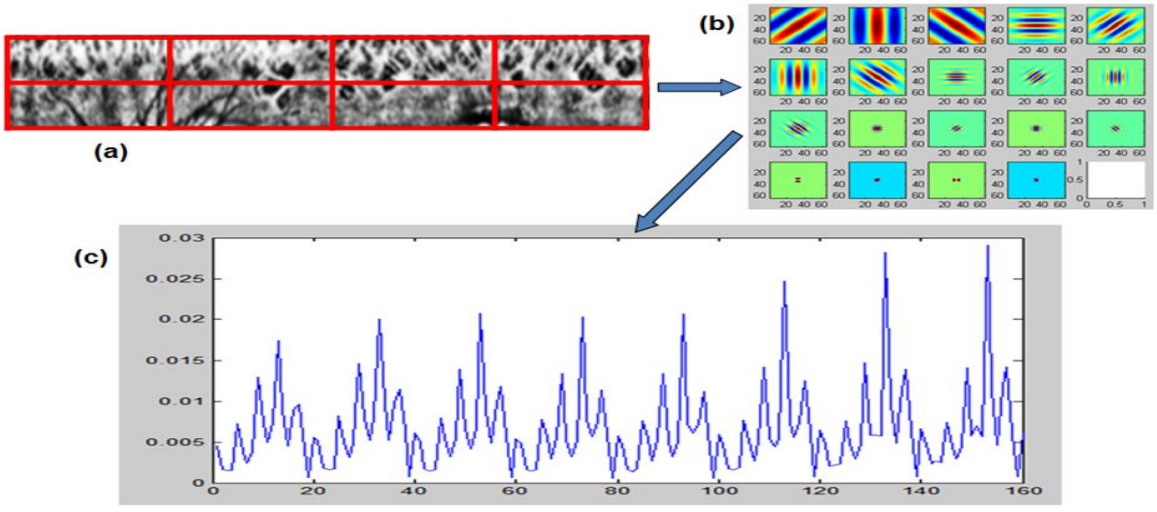

Fig. 10 2D Gabor filter bank based texture feature extraction: (a) Enhanced Normalized Iris Sheet divided into 8 patches; (b) 20 2D Gabor Filters; and (c) Texture feature vector with 160 average absolute deviation (ADD) values

V. Experiment Setup and Results

In this section, we describe the iris databases used to evaluate the performance of our iris recognition system, including both enrollment and matching. Then we summarize the parameters used and present the results for matching.

5.1 Iris Datasets

To evaluate the performance of our iris recognition system, we selected two iris databases, namely CASIA-IrisV1 and CASIA-IrisV3 [5]. They are chosen because the iris images in these databases encompass most of the irregularities caused by different acquisition instruments specification and various acquisition conditions. The databases also contain iris images captured from different ethnicity.

5.2 Experiment Setup and Results

Table1 summarizes the experiment setup we used in the evaluation. These values are used in the evaluation of our iris recognition system, including both enrollment and matching. All parameters were chosen empirically to best fit for iris images from both CASIA-Iris databases. Both the enrollment and matching process use the same iris segmentation and texture feature extraction mechanism described. For enrollment process, after the texture-based feature vector with 160 ADD values is extracted, it will be saved into the database with the original iris image with iris owner identity information. For the matching process, the feature vector will be extracted from the incoming new iris image before similarity value based on Euclidean distance is calculated between the new iris and the feature vector of each of the iris image already in the database. Only the iris image with the highest similarity value will be returned as the matching one.

Figure 11 shows a simple user interface we designed in Matlab to enroll and match the iris. After the iris image files are read into the system, both the enrollment and matching process take little time. Two additional functions are also included in the Matlab application. First, when there is no matching found, enrollment process will be triggered and the user will be prompted to input the iris owner identify information. Secondly, image acquisition capability is included so that in addition to reading iris image from the available database, new iris image can be acquired directly and fed into the iris recognition system to enroll or find matching. This function simulates the real world security scenario where iris images are taken from new individuals that have never been registered in any databases. Figure 11 also shows the iris image acquired directly from a volunteer in the lab using an embedded webcam on a laptop, and the prompt asking the user to "Enter Iris Owner Identity".

Table 1 Parameters used in the Evaluation of Our Iris Recognition System

Para.	Value	Description
N	35	Iris-pupil boundary identification, used in threshold min ($I(x,y)$)+N
R_D	3	Secondary disk radius for dilation operator
R_E	2	Secondary disk radius for erosion operator
r	64	Radius range of radial coordination for normalized iris sheet
θ	512	Angle range of radial coordination for normalized iris sheet
M	16	Window size of low pass Gaussian filter used in image enhancement
m x n	32x64	Patch size on which 2D Gabor filter bank is applied
ϑ	[0 45 90 135]	Four orientations used in 2D Gabor filter bank
f	[0.157, 0.346, 0.691, 1.414, 2.827]	Five central radial frequencies used in 2D Gabor filter bank

Using the dataset chosen from CASIA-IrisVx, our algorithms achieved 100% recognition rate. When the system is tested against iris images acquired directly from volunteers, the recognition rate hovers around 90%, after enrolling the first iris image for the individual. We believe the reduction in the success rate is mainly due to the uncertainty introduced by image quality decline caused by camera settings of embedded webcam on laptop, no control of the ambient lighting and no strict requirements for the pose of the volunteers.

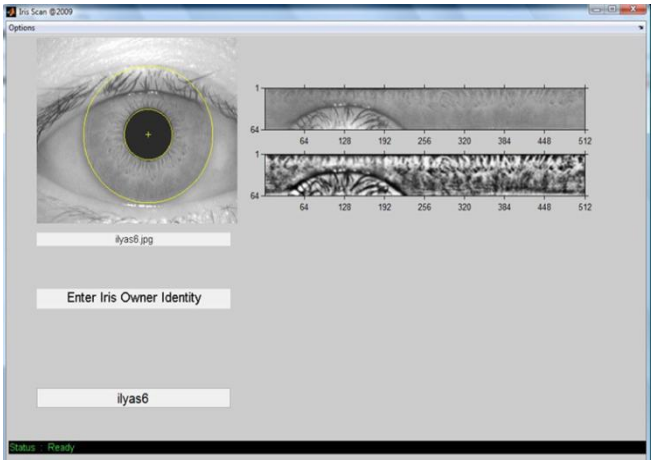

Figure 11 Iris Recognition Implementation in Matlab: IrisScan

VI. Conclusion

In this paper, we presented an iris recognition system based on improved iris segmentation and feature extraction algorithms. Details of iris localization, normalization, enhancement, and texture based feature extraction are presented. Our iris segmentation algorithm shows comparable accuracy as those computationally more intensive algorithms such as Hough and active contour. Our iris recognition system implementation in Matlab, IrisScan, achieved high accuracy with minimum computational time.

A future direction for the iris recognition is to develop algorithms that can provide descent recognition success rate in a timely manner when dealing with iris images taken from moving subjects such as those from security surveillance video.

ACKNOWLEDGEMENT

The authors want to thank the discussion we had with members of the HAVOC (Houston Area Visual Optics Journal Club) at the University of Houston for clinical insights regarding physiology behind iris and with Dr. Xiaohui Yuan from University of North Texas for image segmentation and enhancement methods.

REFERENCES

[1] Y. Adini, Y. Moses, and S. Ullman, "Face recognition: the problem of compensating for changes in illumination direction," IEEE Trans. Pattern Anal. Machine Intell., vol. 19, pp. 721–732, July 1997.

[2] P. N. Belhumeur, J. P. Hespanha, and D. J. Kriegman, "Eigenfaces vs. Fisherfaces: Recognition using class-specific linear projection," IEEE Trans. Pattern Anal. Machine Intell., vol. 19, pp. 711–720, July 1997.

[3] A.K. Jain, R.M. Bolle, and S. Pankanti, Eds., Biometrics: Personal Identification in a networked Society, Norwell, MA: Kluwer, 1999.

[4] G.Gürkan, A. Akan, "Texture Analysis Based Iris Recognition", Istanbul University Journal of Electrical and Electronics Engineering vol. 6, No 1, 2006.

[5] J.Daugman, "How Iris Recognition Works," IEEE Trans. On Circuits and Systems for Video Technology, vol. 14, No. 1 Jan 2004.

[6] K.S.S.Kyaw, "Iris Recognition using features for biometric Identification" IEEE Electronic Computer Technology, pp. 554–556, Feb 2009.

[7] J.Daugman "New Methods in Iris Recognition", IEEE Transaction and System Man and Cybernetics: Part B vol.37 No.5 , October 2007.

[8] H.Zheng, F.Su, "An Improved Recognition System Based on Gabor Filters" IEEE Network Infrastructure and Digital Content, pp. 823–827, Nov 2009.

[9] K. W. Bowyer, K.Hollingsworth, P.J.Flynn "Image Understanding for Iris Biometrics: Survey", Computer Vision and Image Understanding, vol.110 (2), 2008.

[10] R. P.Wildes, "Iris recognition: An emerging biometric technology," Proc. IEEE, vol. 85, no. 9, pp. 1348–1363, Sep. 1997.

[11] L. Ma, T. Tan, Y. Wang, and D. Zhang, "Personal identification based on iris texture analysis," IEEE Trans. Pattern Anal. Mach. Intell., vol. 25, no. 12, pp. 1519–1533, Dec. 2003.

[12] L. Ma, T. Tan, Y. Wang, and D. Zhang, "Efficient iris recognition by characterizing key local variations," IEEE Trans. Image Process., vol. 13, no. 6, pp. 739–750, Jun. 2004

[13] J. Daugman. High confidence visual recognition of persons by a test of statistical independence. IEEE Transactions on Pattern Analysis and Machine Intelligence, Vol. 15, No. 11, 1993.

[14] X. Yuan, Segmentation of Blurry Object by Learning from Examples, SPIE Medical Imaging, San Diego, CA, Feb. 13-18, 2010